Stochastic TEC and Structure Models

Charles Rino

March 7, 2019

Abstract

This report is a detailed development of stochastic TEC structure characterization following a presentation at the February 19-21 St. Augustine, Florida LWAS workshop . We first identify ionospheric structure that admits quantitative stochastic structure characterization. We then introduce a revised three-dimensional ionospheric structure model that can be used to interpret diagnostic TEC measurements.

1 Introduction

Ionospheric structure can cause propagation disturbances that degrade the performance of satellite communication, navigation, and surveillance systems. Physics-based models are being constructed to assess and ultimately predict the structure. Quantitative characterization of the structure is an essential part of this process. This report reviews and extends stochastic structure characterization. Although the ionosphere is an extremely complex system, the electron density observable, $N_e(\mathbf{r}, t)$, is sufficient for both structure characterization and assessment of propagation effects.

Large-scale slowly varying structure is the starting point. To identify large-scale structure formally, let

$$N_e(\mathbf{r}, t) = \overline{N}_e(\Delta\mathbf{r}, \Delta t) + DN_e(\Delta\mathbf{r}, \Delta t). \tag{1}$$

The coordinates $\Delta\mathbf{r}$ and Δt are confined to a region of interest (ROI) centered on reference a GPS coordinate, $\mathbf{r}_0$, and evolving from a reference universal time, t_0. The component $\overline{N}_e(\Delta\mathbf{r}, \Delta t)$ represents a deterministic structure component that can be characterized analytically with physics-based models. Processes that cause systematic variations of $\overline{N}_e(\mathbf{r}, t)$ initiate the development and evolution of residual structure represented by $DN_e(\Delta\mathbf{r}, \Delta t)$. To interpret diagnostic measurements the ROI structure is partitioned as follows:

$$N_e(\Delta\mathbf{r}, \Delta t) \simeq \overline{N}_e(\mathbf{r}_0, t_o) + \Delta N_e(\mathbf{v}_{\rm eff}\,(t - t_0)) + \delta N_e(\Delta\mathbf{r}, \Delta t). \tag{2}$$

The term ΔN_e represents *intermediate-scale* structure that evolves slowly enough to present spatially invariant (frozen) configurations over typical measurement

intervals. The term δN_e represents *small-scale* more rapidly varying spatially dispersive structure.

Different diagnostic measurements emphasize different scale-size components. Ionosondes measure N_e profiles with comparatively coarse resolution. Spread F is a manifestation of intermediate-scale structure, but not a quantitative diagnostic. Similarly, coherent backscatter radars measure the Bragg wavelength component of $\delta N_e(\Delta\mathbf{r}, \Delta t)$ as a time series. Backscatter time series are processes to extract Doppler shifts, which, in turn, measure plasma motion. Incoherent scatter exploits theoretical power spectral density (PSD) predictions to extract electron density, composition, and ion temperature estimates. However, incoherent scatter measurements cannot resolve intermediate-scale structure. Only propagation diagnostics and in-situ probes provide quantitative measures of intermediate-scale structure.

The phase of signals that propagate through disturbed regions are sensitive to path-integrated electron density, which is referred to as total electron content (TEC). TEC is introduced as a mapping of three-dimensional ionospheric structure onto a two-dimensional measurement plane normal to the direction of path integration:

$$TEC(\mathbf{r}_s, t) = \int_0^L N_e(\mathbf{r}, t) ds. \tag{3}$$

Upon neglecting δN_e, TEC can be separated into deterministic and stochastic components as follows:

$$TEC(\mathbf{r}_s, t) = \overline{TEC}(\mathbf{r}_s, t) + \int_0^L \Delta N_e(\mathbf{v}_{\text{eff}}\,(t - t_0)) ds. \tag{4}$$

The velocity $\mathbf{v}_{\text{eff}}$ includes the motion of the path of integration and the drift velocity, which is usually unknown. The remainder of this report will addres stochastic structure characterization.

It is important to note that TEC as represented by (4) applies only to subregions and time intervals that support invariant drifting structure. Intermediate-scale structure does undergo slow rearrangement, which leads to variation within ROIs. Identifying appropriate analysis intervals to capture this variation is part of structure characterization. Small-scale structure within an ROI is intrinsically spatially dispersive. Plasma waves with different scales move with different velocities. Propagation and coherent backscatter measurements are complementary, with causal relations yet to be determined.

2 Stochastic Structure Models

Without loss of generality, the x axis of an ROI coordinate system can be aligned with the ray that connects the phase centers of the transmit and receive antennas. Because of the large GNSS propagation distances and orbital periods, the directions of the paths of integration are nearly invariant over typical measurement intervals. Moreover, although the geometric path is not the strict path

an interrogating electromagnetic wave follows, propagation models based on

$$\Delta TEC(\boldsymbol{\rho}) = \int_0^L \Delta N_e(x, \boldsymbol{\rho}) dx. \tag{5}$$

capture refraction and diffraction.

Stochastic models of intermediate-scale ionospheric structure follow from spectral density functions (SDFs), which are formally ensemble averages of the intensity of Fourier decompositions of the structure. The underlying model is three dimensional. TEC effectively maps the three-dimensional structure onto a two-dimensional observation plane. Any physical structure realization admits the following interrelated three, two, and one-dimensional Fourier decompositions:

$$\widehat{\Delta N}_e(\kappa_x, \boldsymbol{\kappa}) = \int \iint \Delta N_e(x, \boldsymbol{\rho}) \exp\{-i\kappa_x x\} \exp\{-i\boldsymbol{\kappa} \cdot \boldsymbol{\rho}\} d\boldsymbol{\rho} dx \tag{6}$$

$$\widehat{\Delta N}_e(\boldsymbol{\kappa}) = \int \widehat{\Delta N}_e(\kappa_x, \boldsymbol{\kappa}) \frac{d\kappa_x}{2\pi} \tag{7}$$

$$\widehat{\Delta N}_e(\kappa_y) = \iint \widehat{\Delta N}_e(\kappa_x, \kappa_y, \kappa_z) \frac{d\kappa_x}{2\pi} \frac{d\kappa_z}{2\pi} \tag{8}$$

The κ_y SDF is derived from a scan along the y axis. Accommodating an arbitrary scan direction is a purely geometrical manipulation. The formal SDF definition is

$$\Phi_{N_e}^{(n)} = \left\langle \left| \widehat{\Delta N}_e \right|^2 \right\rangle, \tag{9}$$

where $n = 1, 2$, or 3 indicates the dimension. The angle brackets indicate an ensemble average. The following standard procedure is used for generating realizations of $\Delta N_e(x, \boldsymbol{\rho})$:

$$\begin{aligned} \Delta N_e(x, \boldsymbol{\rho}) = & \int \iint \sqrt{\widehat{\Delta N}_e(\kappa_x, \boldsymbol{\kappa})} \xi(\kappa_x, \boldsymbol{\kappa}) \\ & \times \exp\{i\kappa_x x\} \exp\{i\boldsymbol{\kappa} \cdot \boldsymbol{\rho}\} \frac{d\boldsymbol{\kappa}}{(2\pi)^2} \frac{d\kappa_x}{2\pi}, \end{aligned} \tag{10}$$

where $\xi(\kappa_x, \boldsymbol{\kappa})$ is a process with the formal white noise property

$$\begin{aligned} \left\langle \xi(\kappa_x, \boldsymbol{\kappa}) \xi^* \left(\kappa_x', \boldsymbol{\kappa}' \right) \right\rangle = & (2\pi)^2 \delta(\boldsymbol{\kappa} - \boldsymbol{\kappa}') \\ & \times 2\pi \delta\left(\kappa_x - \kappa_x' \right). \end{aligned} \tag{11}$$

One can show that SDFs of the realizations support the interrelated multidimensional SDFs.

To calculate the two-dimensional Fourier decomposition of $\Delta TEC(x, \boldsymbol{\rho})$, $\Delta N_e(x, \boldsymbol{\rho})$ in (5) is replaced with its three-dimensional Fourier representation to obtain the equivalent representation

$$\Delta TEC(x, \boldsymbol{\rho}) = \int \left[\iint \widehat{\Delta N}_e(\kappa_x, \boldsymbol{\kappa}) \exp\{i\boldsymbol{\kappa} \cdot \boldsymbol{\rho}\} \frac{d\boldsymbol{\kappa}}{(2\pi)^2} \right] \exp\{i\kappa_x x\} \frac{d\kappa_x}{2\pi}. \tag{12}$$

Computing the ensemble average of the two-dimensional Fourier transform of (12), using the white-noise property, and evaluaing the integral over x produces the following result

$$\Phi_{\Delta TEC}\left(\boldsymbol{\kappa}\right) = L\int_{-\infty}^{\infty}\frac{\sin^2(\kappa_x L/2)}{(\kappa_x L/2)^2}\Phi_{N_e}\left(\kappa_x,\boldsymbol{\kappa}\right)\frac{d\kappa_x}{2\pi}, \tag{13}$$

which is the primary relation for interpreting diagnostic stochastic TEC measurements. An analytic representation of $\Phi_{N_e}\left(\kappa_x,\boldsymbol{\kappa}\right)$ is needed to pursue the ramifications of (13), .

2.1 The Shakorofsky SDF Model

An analytic model proposed by Shakorofsky has been used extensively for isotropic power-law processes such as Kolmogorov turbulence. The Shakorofsky model is discussed in detail in Section 3.1.4 of Rino [1]. With a change from refractive index units to electron density units, the three-dimensional SDF is

$$\Phi_{N_e}\left(q\right) \sim C_s(q_L^2 + q^2)^{-(\nu+1/2)}, \tag{14}$$

where q_L is the outer-scale spatial wavenumber in radians per meter. The structure function has the complementary power-law form

$$\left\langle\left(\Delta N_e(\zeta) - \Delta N_e(\zeta + y)\right)^2\right\rangle \tilde{} C_n^2 y^{2\nu-2}. \tag{15}$$

Asymptotic equivalence here means the variables q and y are confined to complementary power-law ranges bounded by the outer scale or $2\pi/q_0$. There is no formal dependence on an inner scale cutoff as long as the spectral index parameter $\nu > 1$.

Structure functions are used because they mitigate trend-like departures from strict statistical homogeneity. For example, it can be shown that

$$C_n^2 = \frac{2\Gamma(2-\nu)C_s}{(4\pi)^{3/2}(\nu-1)\Gamma(\nu+1/2)2^{2\nu-2}}, \tag{16}$$

which is independent of the outer scale. For Kolmogorov turbulence $\nu = 4/3$, whereby the structure constant provides a scale-independent measure of turbulent strength. Even so, parameter estimation based on measured PSDs provide a more general hypothesis test.

If the SDF structure contributing to (13) is decorrelated over the path distance L, $\Phi_{N_e}\left(\boldsymbol{\kappa}\right) \simeq \Phi_{N_e}\left(0,\boldsymbol{\kappa}\right)$. It then follows that

$$\Phi_{\Delta TEC}\left(\kappa\right) \sim LC_s(q_L^2 + \kappa^2)^{-(\nu+1/2)}, \tag{17}$$

which suggests that the two-dimensional TEC structure is a direct mapping of the three-dimensional electron density structure with one spatial wavenumber

component set equal to zero. If the structure is correlated over distances greater than L, the approximation

$$\Phi_{\Delta TEC}\left(\boldsymbol{\kappa}\right) \simeq L \int_{-\infty}^{\infty} \Phi_{N_e}\left(\kappa_x, \boldsymbol{\kappa}\right) \frac{d\kappa_x}{2\pi}. \tag{18}$$

is more appropriate. The differences are manifest in the relation between the in situ and one-dimensional SDF spectral index relations. One might expect a wavelength-dependent change in the spectral index.

2.2 Anisotropy

The simplicity of the isotropic model is appealing. However, ionospheric structures are highly anisotropic. Following a procedure introduced by Richard Singleton, anisotropy can be accommodated by replacing q with the generalized quadratic form

$$q^2 = \boldsymbol{q}^T \widehat{\widehat{C}} \boldsymbol{q}, \tag{19}$$

where $\widehat{\widehat{C}}$ is a 3×3 unitary matrix characterizing a rotation from $\boldsymbol{\zeta}$ to a field-aligned system stretched along two directions represented by vectors aligned with and normal to the magnetic field. The elements of $\widehat{\widehat{C}}$ are define in Appendix A.3 of Rino [1]. The complete TEC model depends on the parameters LC_s, ν, the direction of the magnetic field in the reference coordinate system, a field-aligned elongation factor, a, a cross-field elongation factor, b, and the angle of the cross-field elongation plane, γ. Aside from the SDF dependence on q_L, Shakarofosky-Singleton is formally a two-parameter model defined by LC_s and ν, with an implicit dependence on the direction of the magnetic field, elongation ratios, and an orientation angle of the propagation path relative to the magnetic field direction.

3 Configuration-Space SDF Models

Simulations driven by propagation models are limited mainly by the fidelity of structure models. However, structure realizations based on (10) are mathematical abstractions with no direct connection to the underlying physics. Moreover, large-scale realizations require three-dimensional Fourier decompositions over the entire defining volume. In effect every spectral domain sample potentially effects every point in the realization. In a recently paper, Rino et al. [2], we proposed an alternative model that generates stochastic structure realizations as summations of elemental field-aligned *striations*. Striations characterize the ionization associated with individual magnetic field lines. A configuration-space realization replaces (10) with

$$\Delta N_e(x, \boldsymbol{\rho}) = \frac{1}{N_s} \sum_{k=1}^{N_s} C_k \sigma_k^{\gamma_k} p_\perp \left(\sqrt{\left(s + \eta_{S_k}\right)^2 + \left(t + \eta_{S_k}\right)^2} / \sigma_k \right). \tag{20}$$

The profile function $p_\perp(\rho)$, which is zero for $\rho > 1$ with $p_\perp(0) = 1$, defines the radial decay of the striation ionization or its exclusion. The parameters C_k, σ_k, and γ_k define the peak intensity, $C_k\sigma_k^{\gamma_k}$, and scale σ_k, of the k^{th} striation. The parameters η_{S_k} and η_{S_k} identify magnetic field lines from their intercept in a field-aligned coordinate system with s and t measured in a plane normal to the magnetic field direction. The defining coordinates $[x, \boldsymbol{\rho}]$ are transformed into the field-aligned system using the same 3×3 rotation matrix than defines $\overline{C}$ with $a = b = 1$. This version of the configuration-space model assumes no variation along the field lines within the realization volume. To the extent that field-aligned variations can be modeled, the variation be accommodated by introducing a second field-aligned profile function. Field line curvature can also be incorporated with magnetic-field-line tracing.

3.1 Configuration Space Parameter Selection

Configuration parameter selection requires a theoretical computation of the expectation SDF. However, because the model admits no stochastic variation along field lines, stochastic structure can be characterized only in cross-field planes. Consider a realization with the x axis aligned with the magnetic field. A formal calculation of the multi-dimensional SDF will show that

$$\Phi_{\Delta N_e}(\kappa_x, \boldsymbol{\kappa}) = \frac{1}{N_s}\sum_{j=1}^{J} N_j \sigma_j^{2\gamma_j+(2-\varepsilon(n))} C_j^{(n)} Q^{(n)}(\kappa_x, \boldsymbol{\kappa}; \sigma_j) \tag{21}$$

$$Q^{(n)}(\kappa_x, \boldsymbol{\kappa}; \sigma_j) = \left| \int \cdots \int p_\perp\left(\sqrt{s^2+t^2}/\sigma_j\right) \exp\{-i\left(x\kappa_x + \boldsymbol{\kappa}\cdot\boldsymbol{\rho}\right)\} dy d\boldsymbol{\rho} \right|^2, \tag{22}$$

where $\varepsilon(n)$ is a correction that will be discussed shortly. The derivation of (21) and (22) follows the development in Rino et al. [2], where only the one-dimensional SDF was used. From (21), SDFs are defined by the parameters J, N_j, σ_j, γ_j, and C_j. The parameters J and N_j partition the striations into J groups of N_j striations, whereby

$$N_s = \sum_{j=1}^{J} N_j. \tag{23}$$

A defining relation is most readily established by using the measurable one-dimensional SDF

$$\Phi_{\Delta N_e}(\kappa_y) = \frac{1}{N_s}\sum_{j=1}^{J} N_j \sigma_j^{2\gamma_j+\epsilon(1)} C_j Q^{(1)}(\kappa_y; \sigma_j) \tag{24}$$

$$Q^{(1)}(\kappa_y, \sigma_j) = \left| \int p_\perp\left(\sqrt{s^2+t^2}/\sigma_k\right) \exp\{-iy\kappa_y\} dy \right|^2. \tag{25}$$

Realizations are constrained to approximate one-dimensional target SDFs of the form

$$\Phi_{\Delta N_e}(\kappa_y) = C_p \begin{cases} \kappa_y^{-\eta_1} & \text{for } \kappa_y \le \kappa_0 \\ \kappa_0^{\eta_2-\eta_1}\kappa_y^{-\eta_2} & \text{for } \kappa_y > \kappa_0 \end{cases} . \tag{26}$$

This is achieved by imposing the following bifurcation rule:

$$\sigma_j = \sigma_{\max} 2^{-(J_{\max}-j)} \quad j = 1, 2, \cdots J_{\max} \tag{27}$$

$$N_j = 2^{d-J_{\max}} \tag{28}$$

Bifurcation means that each new scale is half the next larger scale. We find that with $\epsilon(1) = 1$, the desired expectation SDF is realized with

$$\eta_{1,2} = 2\gamma_{1,2} + 2. \tag{29}$$

The index subscript refers to the large-scale, $\kappa_y \le \kappa_0$, and small-scale, $\kappa_y > \kappa_0$, spatial wavenumber ranges.

A specific realization is initiated by defining $\sigma_{\max}$, which corresponds to the smalles power-law wavenumber , $2\pi/\sigma_{\max}$. Similarly, $J_{\max}$ defines the smallest striation scale $\sigma_1 = \sigma_{\max} 2^{-(J_{\max}-1)}$, which corresponds to the largest power-law spatial wavenumber, $2\pi/\sigma_1$. Initially let $d = J_{\max}$, which assigns one striation to bifurcation. The set of J logarithmically-spaced wavenumbers comprise a discrete wavelet decomposition, as discussed in [3] and [4]. The C_j parameter defines C_p with an adjustment at the break frequency for to maintain SDF continuity. Figure 1 shows a comparison of a target SDF (blue) with and the expectation SDF computed by evaluating (24) with $\sigma_{\max} = 20$ km, $J_{\max} = 10$ and the remaining parameters identified in the plot title.

Parameters can be adjusted to identify the smallest value of J that provides good definition over the target SDF range. The departure of the expectation SDF at the low frequency end in Figure 1 is the Fourier transform of the largest striation, $Q^{(1)}(\kappa_y, \sigma_J)$. The high frequency departure is determined similarly by $Q^{(1)}(\kappa_y, \sigma_j)$. If Δy is small enough, the sidelobes of the smallest striation become visible. For larger values there is some aliasing, which accounts for the upward departure in Figure 1. The resolution, Δy, determines the minimum cross-field sampling in a plane normal to the magnetic field that will support the SDF. The parameter $d \ge J$ determines the total number of striations, which must be large enough to provide a uniform distribution of striations threading the ROI. The contributions from adjacent field lines overlap.

An overall adjustment to $C_j^{(1)}$ has been applied to match the target SDF. For the two-dimensional SDF we find that the relation

$$\Phi^{(1)}_{\Delta N_e}(\kappa_y) = \int \Phi^{(2)}_{\Delta N_e}(\kappa_y, \kappa_x) \frac{d\kappa_x}{2\pi} \tag{30}$$

is realized with $\epsilon(2) = 2$ with a similar overall adjustment to $C_j^{(2)}$ to maintain full consistency. The upper frame in Figure 2 shows shows a color display of

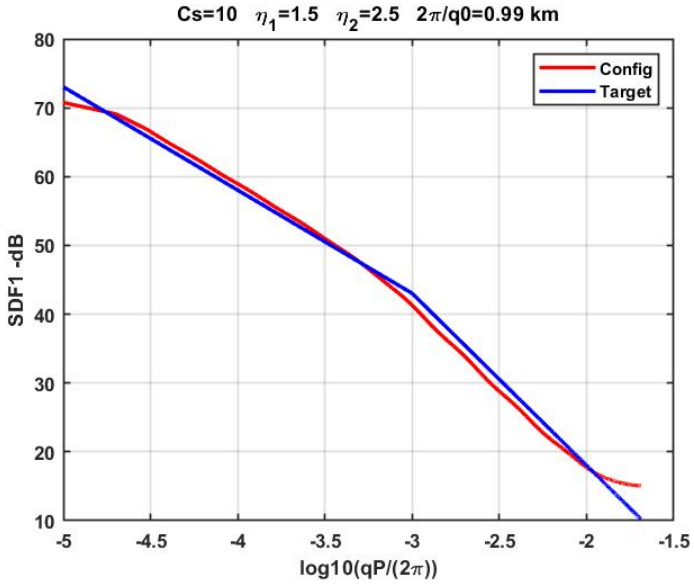

Figure 1: Target SDF for parameters listed in the title (blue) overlaid on the SDF computed from (24).

$\Phi^{(2)}_{\Delta N_e}(\kappa_y, \kappa_z)$, which corresponds to field-aligned propagation. The blue plot in the lower frame is obtained by integrating $\Phi^{(2)}_{\Delta N_e}(\kappa_y, \kappa_z)$ over κ_z. The red curve is the one-dimensional SDF $\Phi^{(1)}_{\Delta N_e}(\kappa_y)$ shown in Figure 1 as a check on the calculation and normalization. Although (22) provides a complete characterization of the configuration space structure, it is desirable to have an analytic representation. We find that

$$\Phi_{\Delta N_e}(\kappa_y, \kappa_z) = C_s^2 \begin{cases} \kappa^{-p_1} & \text{for } \kappa \le \kappa_0 \\ \kappa_0^{p_2-p_2}\kappa^{-p_2} & \text{for } \kappa > \kappa_0 \end{cases}, \tag{31}$$

with $p_n = \eta_n + 1$ provides a good fit to $\Phi^{(2)}_{\Delta N_e}(\kappa_y, \kappa_z)$. This is illustrated in Figure 3 where the where $\Phi_{\Delta N_e}(\kappa)$ as defined by (31) is overlaid on the expectation calculation. For each calculation consistent scaling is maintained to connect the two-dimensional model C_s^2 to the defining value one-dimensional C_s value.

At this point, a one-dimensional scan of an ROI could be processed with irregularity parameter estimation (IPE) as described in Rino and Carrano [4] to extract the one-dimensional parameters, which can be related directly to the two-dimensional cross-field defining relation. To interpret a stochastic TEC measurement, (13) must be evaluated, which requires a three-dimensional SDF model.

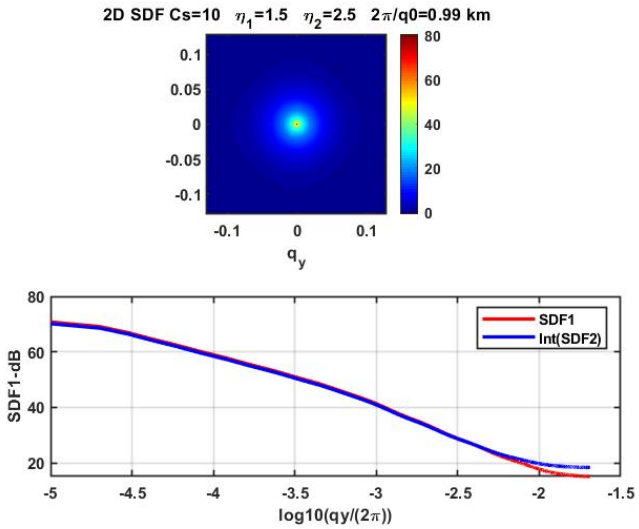

Figure 2: Upper frame is two-dimensional SDF computed from (22) with $n = 2$. Lower frame is calculation of one-dimensional SDF by integration (blue) overlaid on expectation SDF (red).

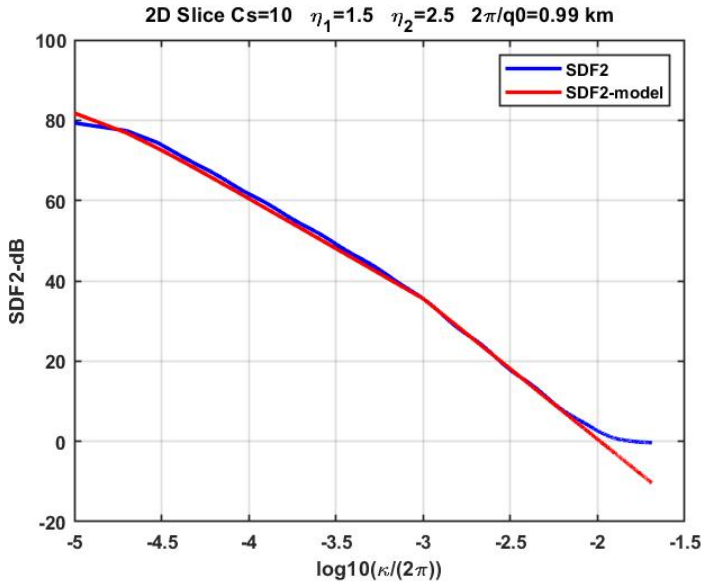

Figure 3: Comparison of analytic two-dimensional model (red) from (31) with expectation calculation from (22) with $n = 2$.

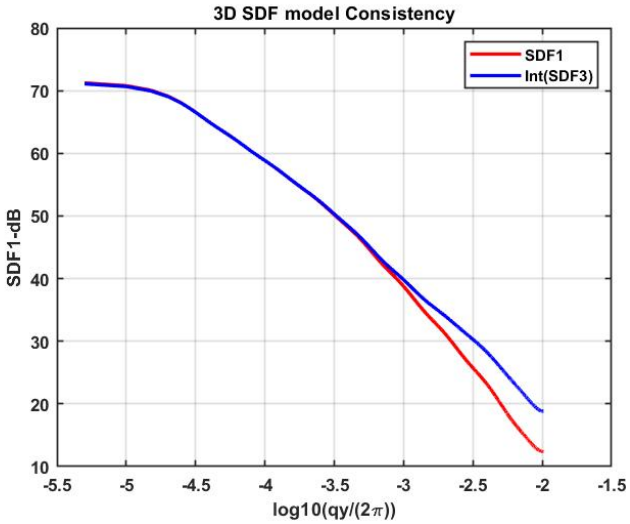

3.2 Extension to Three Dimensions

Upon computing $\Phi_{\Delta N_e}(\kappa_x, \kappa_y, \kappa_z)$ as defined by (21) and comparing the expectation one-dimensional result () to

$$\Phi^{(1)}_{\Delta N_e}(\kappa_y) = \iint \Phi^{(3)}_{\Delta N_e}(\kappa_y, \kappa_x, \kappa_z) \frac{d\kappa_x}{2\pi} \frac{d\kappa_z}{2\pi}, \tag{32}$$

we find that $\epsilon(3) = 2$ maintains consistency. The reason that $\epsilon(3) = \epsilon(2)$ follows from the calculation

$$\begin{aligned} Q^{(3)}(\kappa_x, \boldsymbol{\kappa}; \sigma_j) &= \left| \iint p_\perp \left(\sqrt{y^2 + z^2}/\sigma_j \right) \right. \\ &\quad \left. \exp\{-i\,(y\kappa_y + z\kappa_z)\} dy dz \right|^2 2\pi\delta(\kappa_x). \end{aligned} \tag{33}$$

The numerical calculations approximate singular singular behavior. For example, Figure xx show numerical evaluation of (33) with (21) substituted for $\Phi^{(3)}_{\Delta N_e}(\kappa_y, \kappa_x, \kappa_z)$ with the one-dimensional expectation SDF overlaid. We expect that better agreement could be realized with finer sampling, which makes the computation time-consuming. Unfortunately there is no analytic counterpart to (31).

References

[1] Charles L. Rino. *The Theory of Scinillation with Applications in Remote Sensing*. John Wiley and Sons, 2011.

[2] C. L. Rino, C. S. Carrano, K. M. Groves, and T. Yokoyama. A configuration space model for intermediate scale ionospheric structure. *Radio Sci.*, 53:1–9, 2018. doi:10.1029/2018RS006678.

[3] C. Rino, C. Carrano, K. Groves, and P. Roddy. Wavelet-based analysis and power law classification of C/NOFS high-resolution electron density data. *Radio Sci.*, 49:680âĂŞ688, 2014. doi:10.1002/2013RS005272.

[4] C. L. Rino and C. S. Carrano. On the characterization of intermediate-scale ionospheric structure. *Radio Sci.*, 53:1–12, 2018. 10.1029/2018RS006709.